The Association of Tropical and Extratropical Climate Modes to Atmospheric Blocking across Southeastern Australia

TIM COWAN, PETER VAN RENSCH, ARIAAN PURICH, AND WENJU CAI

CSIRO Wealth from Oceans National Research Flagship, CSIRO Water for a Healthy Country Flagship, Centre for Australian Weather and Climate Research, and CSIRO Marine and Atmospheric Research, Aspendale, Victoria, Australia

(Manuscript received 30 October 2012, in final form 19 March 2013)

ABSTRACT

Relationships of the Indian Ocean dipole (IOD), El Niño–Southern Oscillation (ENSO), and the southern annular mode (SAM) with atmospheric blocking are investigated using a linear framework over the austral autumn–spring (cool) seasons for southeast Australia (SEA). Positive blocking events occurring at 130°–140°E increase the likelihood of cutoff low pressure systems developing that generate significant rainfall totals across SEA. In mid to late austral autumn (April–May), blocking is coherent with negative IOD events. During this season, a negative IOD event and blocking are associated with warm sea surface temperature anomalies in the eastern tropical Indian Ocean and a blocking high pressure cell south of Australia. An anomalous cyclonic pressure center over southern Australia directs tropical moisture flux anomalies to the region. Despite this, only a small portion of a negative IOD's impact on SEA rainfall comes through blocking events. During austral winter, ENSO is coherent with blocking; anomalous tropical moisture fluxes from the western Pacific during a La Niña merge with anomalous cyclonic flows centered over SEA, delivering enhanced rainfall via cutoff lows. The low pressure cell constitutes a center of the Southern Oscillation associated with ENSO. This ENSO-blocking coherence is considerably weaker in austral spring, whereby circulation anomalies associated with blocking resemble a SAM-like pattern. As such, a large portion of the SAM's impact on SEA spring rainfall occurs in conjunction with blocking events. The relative importance of associations between the dominant climate modes and blocking in generating the drought-breaking cool season precipitation in 2010 across SEA is discussed.

1. Introduction

Interannual rainfall variability across southeast Australia (SEA; south of 33°S, east of 135°E; region shown in Fig. 1a) is modulated by three dominant remote climate variability modes: the Indian Ocean dipole (IOD), El Niño–Southern Oscillation (ENSO), and the southern annular mode (SAM) (e.g., McBride and Nicholls 1983; Nicholls et al. 1996; Ashok et al. 2003; Cai and Cowan 2006; Murphy and Timbal 2008; Risbey et al. 2009b; Cai et al. 2009; Hill et al. 2009; Nicholls 2010; Cai et al. 2011a,c; Ummenhofer et al. 2011; Pui et al. 2012). The former two climate modes reflect a tropical influence that extends to southern Australian latitudes in the austral winter [June–August (JJA)] and spring [September–November (SON)] seasons, although the IOD can develop in mid to late austral autumn (Du et al. 2013). The teleconnection of IOD events to SEA occurs via equivalent barotropic Rossby wave trains emanating from the tropical Indian Ocean (Cai et al. 2011c; Timbal and Hendon 2011). Wave trains, triggered by convection anomalies in the tropical Indian Ocean, induce a high pressure anomaly downstream to the south of Australia, which can modify the intensity and position of the local subtropical ridge (Cai et al. 2011b; Timbal and Hendon 2011). This, in turn, can lead to a displacement of the midlatitude westerlies that affect the likelihood of precipitation over the region (Cai et al. 2011c). Likewise, ENSO generates an extratropical wave train response emanating from the tropical Pacific Ocean; in the Southern Hemisphere (SH) this is described as the Pacific–South American (PSA) pattern (Karoly 1989). However, because the mean location of this PSA pattern is well to the east of Australia, it does not play a role in generating precipitation over southern Australia during the winter and spring months (Cai et al. 2011c). The impact of ENSO on tropical Australia in winter occurs through the Southern Oscillation (SO)

Corresponding author address: Tim Cowan, CSIRO Marine and Atmospheric Research, PMB 1, Aspendale, Victoria 3195, Australia. E-mail: tim.cowan@csiro.au

DOI: 10.1175/JCLI-D-12-00781.1

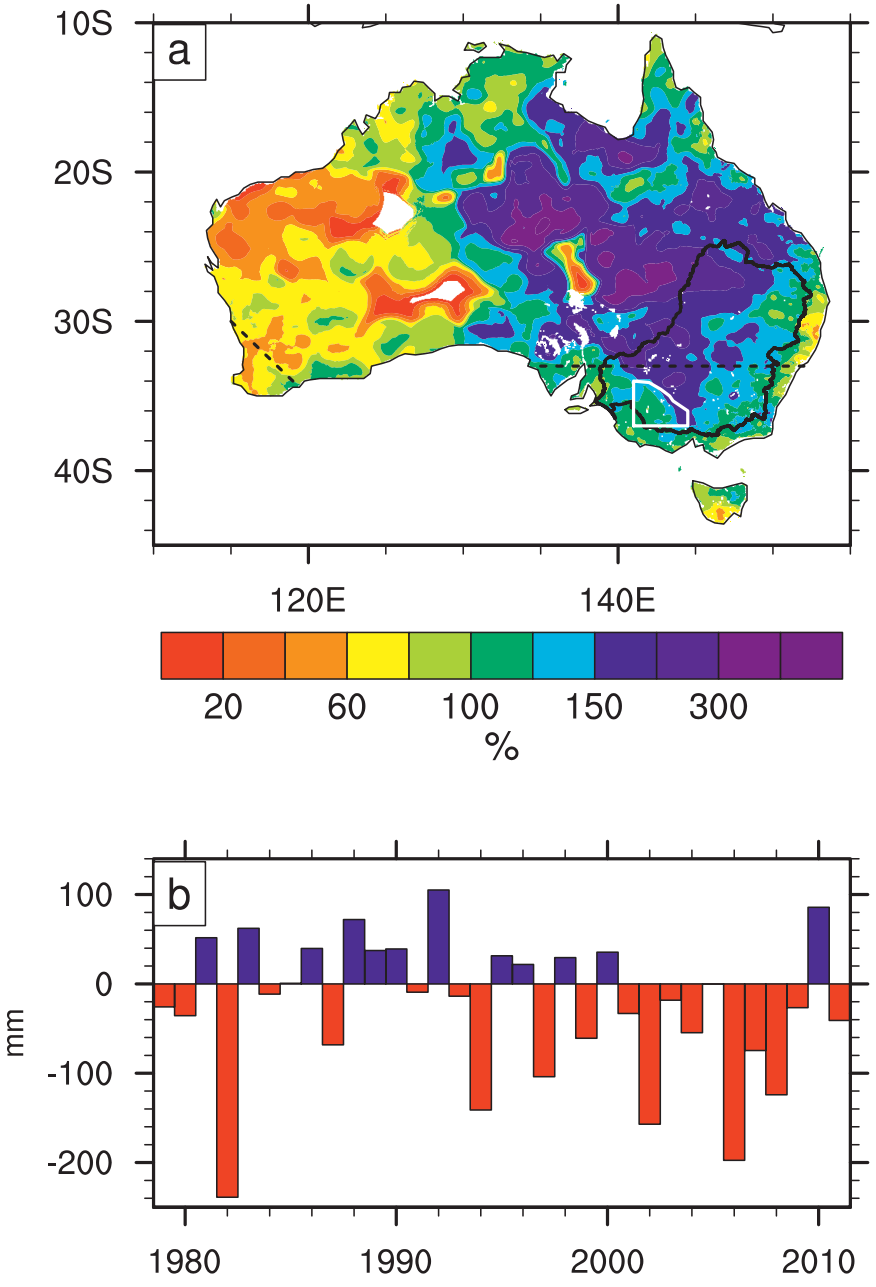

FIG. 1. (a) Cool season (April–November) rainfall for 2010 as a percentage of 1971–2000 climatology and (b) time series of area-averaged cool season rainfall anomalies for southeast Australia (SEA) for 1979–2010. The regions of southwest Western Australia (diagonal dashed black line), SEA (region south of horizontal dashed black line), the Murray-Darling basin (area enclosed by bold black line), and the Mallee (area outlined in white) are shown in (a). The white regions in central/western Australia in (a) indicate where there is a sparsity of data (e.g., Ummenhofer et al. 2011).

and a weak equivalent-barotropic wave train pattern (Karoly 1989), while in spring ENSO projects its signal to the extratropics and SEA through the tropical Indian Ocean (Cai et al. 2011c).

The most dominant climate mode of variability in the SH extratropics is the SAM, describing the zonal pressure fluctuations between high and midlatitudes (e.g., Thompson and Wallace 2000; Arblaster and Meehl 2006), as well as meridional shifts in zonal winds across these latitudes (Risbey et al. 2009b). Positive SAM events are associated with anomalously dry conditions across southeast and southwest Australia (refer to Fig. 1a for

region location) in winter (Cai et al. 2003; Cai and Cowan 2006; Hendon et al. 2007; Meneghini et al. 2007): in 2010 southwest Australia experienced its driest April–November (cool season) on record (precipitation was 42% below the 1971–2000 average), coinciding with the highest positive SAM in 50 years of records (Cai et al. 2011a). For southern and eastern Australia, the 2010 cool season was anomalously wet (Fig. 1a), with SEA April–November rainfall almost 20% above the long-term average (Fig. 1b). The relationship between SAM and the position of extratropical storm tracks is thought to have contributed to this rainfall response. In recent decades the storm tracks have shifted poleward (Yin 2005) and reduced in intensity (Frederiksen and Frederiksen 2007). This shift has been linked to increasing levels of atmospheric greenhouse gases (Cai et al. 2003; Hope et al. 2006), which act to reduce the vertical mean meridional temperature gradient in the midlatitudes (Cai et al. 2003; Frederiksen and Frederiksen 2007). The position of storm systems is also related to synoptic-scale processes such as atmospheric blocking events, which despite recent advances are still not well understood (e.g., Brown et al. 2009; Risbey et al. 2009a).

Atmospheric blocking describes a process whereby the upper-tropospheric westerly airstream is split into two branches, allowing for either 1) the ''blocking'' of approaching cold fronts, or 2) the cutting off of low pressure systems (Risbey et al. 2009a,b). Depending on the nature and location of blocking, southern Australia can experience anomalously dry or wet conditions (Pook and Gibson 1999; Pook et al. 2006, 2009). Because of their relative small spatial scale, blocking events still remain difficult to simulate in climate models (Pook et al. 2010), so undertaking process-based studies remains a difficult task. Risbey et al. (2009a) found a strong association between cutoff low pressure systems and atmospheric blocking, the latter of which, in turn, was found to be linked to the presence of a positive SAM-like pattern. They found that enhanced atmospheric blocking to the southeast of Australia (~160°E) is favorable for the development of cutoff low pressure systems, while weaker blocking in the Tasman Sea region is associated with drier conditions over much of Australia. However, a comprehensive assessment on how climate modes project their signal onto blocking has yet to be undertaken.

To this end, we investigate the covariability of the large-scale climate modes with an index that describes atmospheric blocking in the context of SEA's cool season climate (i.e., the seasons in which SEA receives ~75% of its rainfall). We acknowledge the fact that blocking events predominantly occur on a weekly temporal scale (Trenberth and Mo 1985); therefore, it is the large protracted events and/or a series of events that contribute to seasonal anomalies. This study investigates how the IOD, ENSO, and SAM interact with atmospheric blocking in the autumn, winter, and spring seasons, and thus exert an impact on SEA rainfall. The remainder of this study is set out as follows. Section 2 details the datasets used and applied methodology, while sections 3 and 4 describe the regime in mid to late austral autumn (April–May) and winter, respectively. Section 5 explores the spring season, including the highly unusual climatic conditions that prevailed across southern and eastern Australia during the spring of 2010. Section 6 summarizes the findings.

2. Data and methods

a. Datasets

The study area of interest is mainly restricted to SEA (see Fig. 1a for region) and the surrounding oceans. Data are analyzed over the period 1979–2010 as the availability of satellite measurements reduces the potential for biases and gaps in reanalysis products (e.g., Thompson and Solomon 2002). We calculate our ENSO and IOD indices from sea surface temperature (SST) data from the Hadley Centre Sea Ice and Sea Surface Temperature (HadISST) global reanalysis dataset (Rayner et al. 2003). To assess the anomalous circulation associated with blocking and the climate modes, mean sea level pressure (MSLP), moisture flux (vertically integrated from the surface to 500 hPa), and upper tropospheric (200 hPa) geopotential height (Z_{200}) are used from reanalysis from the National Centers for Environmental Prediction (NCEP)–National Center for Atmospheric Research (NCAR) (Kalnay et al. 1996). To explore the impact on Australian rainfall we utilize a monthly gridded precipitation dataset at a resolution of 0.05° × 0.05° from the Australian Bureau of Meteorology (Jones et al. 2009).

b. Classification of climate modes and atmospheric blocking

We make use of commonly used indices to describe the remote climate modes, as in Cai et al. (2011b): for ENSO, we use the Niño-3.4 index (SST anomalies averaged over 5°S–5°N, 170°–120°W). While the Southern Oscillation index (SOI), defined as the standardized anomaly of the MSLP difference between Tahiti and Darwin, is often used to describe ENSO variability from an atmospheric perspective, the associated MSLP pattern associated with Niño-3.4 resembles the SO in the cool season (see Figs. 3 and 6 in Cai et al. 2011c); therefore we only focus on Niño-3.4. The IOD is measured through the dipole mode index (DMI), which describes the difference in SST anomalies averaged over the western tropical

Indian Ocean (10°S–10°N, 50°–70°E) and eastern IOD region (10°S–equator, 90°–110°E) (Saji et al. 1999). The SAM index (SAMI) used is that described by Marshall (2003), which is a nonnormalized station-based index of the zonal MSLP between 40° and 65°S. An atmospheric blocking index is defined following the definition of Wright (1994), which uses the mean 500-hPa zonal wind U at subtropical and extratropical latitudes. A blocking index B at a given longitude is defined as

$$B = 0.5(\mathrm{U25°S} + \mathrm{U30°S} + \mathrm{U55°S} + \mathrm{U60°S} - \mathrm{U40°S} - \mathrm{U50°S} - 2 \times \mathrm{U45°S}). \quad (1)$$

This blocking definition describes the split of the westerly jet into two distinct branches: a subtropical jet at 25°–30°S and a polar jet at 55°–60°S (Grose et al. 2012). The magnitude of this split can be represented by the blocking index B, with positive values describing the formation of high (low) pressure cells in the high-latitude (midlatitude) regions (Trenberth and Mo 1985), which are strongly related to precipitation conditions over southern Australia. Blocking conditions are closely related to the number of days with cutoff low pressure systems in the southern Australian cool season, making it a useful tool for process-based studies (e.g., Pook and Gibson 1999; Pook et al. 2006; Risbey et al. 2009b; Pook et al. 2010).

c. Methodology to remove covariability

For this study, complete and partial regression (or correlation) are used to isolate the independent signal of a climate mode from another process [see Cai et al. (2011c) for a detailed description]. Partial regression involves calculating the linear dependence of a mode (e.g., SAMI) upon a process (e.g., rainfall) after the linear relationship between the two and another mode (e.g., blocking at 140°E; B140) has been removed. For example, we can remove the dependency of B140 on the relationship between rainfall and the SAMI by removing the covarying linear coherence between B140 and SAMI, and B140 and rainfall, and then regressing the two residual indices (e.g., $\mathrm{SAMI}|_{\mathrm{B140}}$). This process has been successfully used in previous studies to elucidate the impact of ENSO and IOD on SEA seasonal rainfall (Nicholls 1989; Ashok et al. 2003; Risbey et al. 2009b; Timbal and Hendon 2011; Cai et al. 2011b,c). A potential limitation of this method is the assumption that the observed relationships are linear in nature, when nonlinearities in the teleconnections have been observed (Ummenhofer et al. 2011; Cai et al. 2012; Cai and van Rensch 2013). The method of compositing exceptional blocking years (based on the blocking index passing a given threshold) was used to test the validity of the linear regression method (which uses all data samples). The differences between the two analysis methods were small; therefore, the results of this study are based on regression and partial regression analysis—an investigation of the asymmetry is beyond the scope of this study. Prior to partial regression, all data are first linearly detrended to remove the potential for multidecadal trends to influence interannual relationships. We explore the individual seasons that make up the southern Australian cool season; these are crucial for agricultural industries across SEA, which encompasses the nation's food bowl: the Murray-Darling basin (see Fig. 1a for region location). For this purpose we focus on April–May, JJA, and SON separately, allowing the isolation of distinct seasonal signals. We display circulation–rainfall patterns in terms of the one-standard-deviation anomaly associated with the mode or blocking index—this allows a comparison of the size of anomalies associated with the interannual variability of the climate indices. Statistical significance of the regression coefficients are based on the p value associated with the correlation coefficients (Pearson). We also tested the sensitivity of the relationships using a nonparametric test of correlation (Spearman rank correlation), and found the differences in the correlations to be minimal. The direction of the SEA rainfall response corresponding to negative Niño-3.4 and DMI values (e.g., La Niña and negative IOD conditions) is the same as the direction of rainfall response corresponding to positive blocking values (and cutoff low formation); hence to account for this, the regressions/correlations involving Niño-3.4 and DMI are multiplied by −1.

3. April–May anomalies

Observations show that SEA has experienced a substantial rainfall reduction since the 1980s during autumn (Murphy and Timbal 2008; Cai and Cowan 2008a; Cai et al. 2011b; Cai and Cowan 2013), effectively ''turning off'' the autumn wetting mechanism (Cai and Cowan 2008b), which has serious consequences for the start of the growing season across southern Australia (Pook et al. 2006, 2009). To understand the spatial evolution of the impact of the position of a blocking anticyclone on variability across SEA in April–May, we examine MSLP and Australian rainfall anomalies associated with blocking at different longitudes (Fig. 2).

It is immediately clear that the local pressure and rainfall response across southern Australia is sensitive to the location of the blocking high. In the 120°–140°E band, atmospheric blocking (assuming positive B values) is associated with a high pressure anomaly center to the south of the Great Australian Bight and anomalously

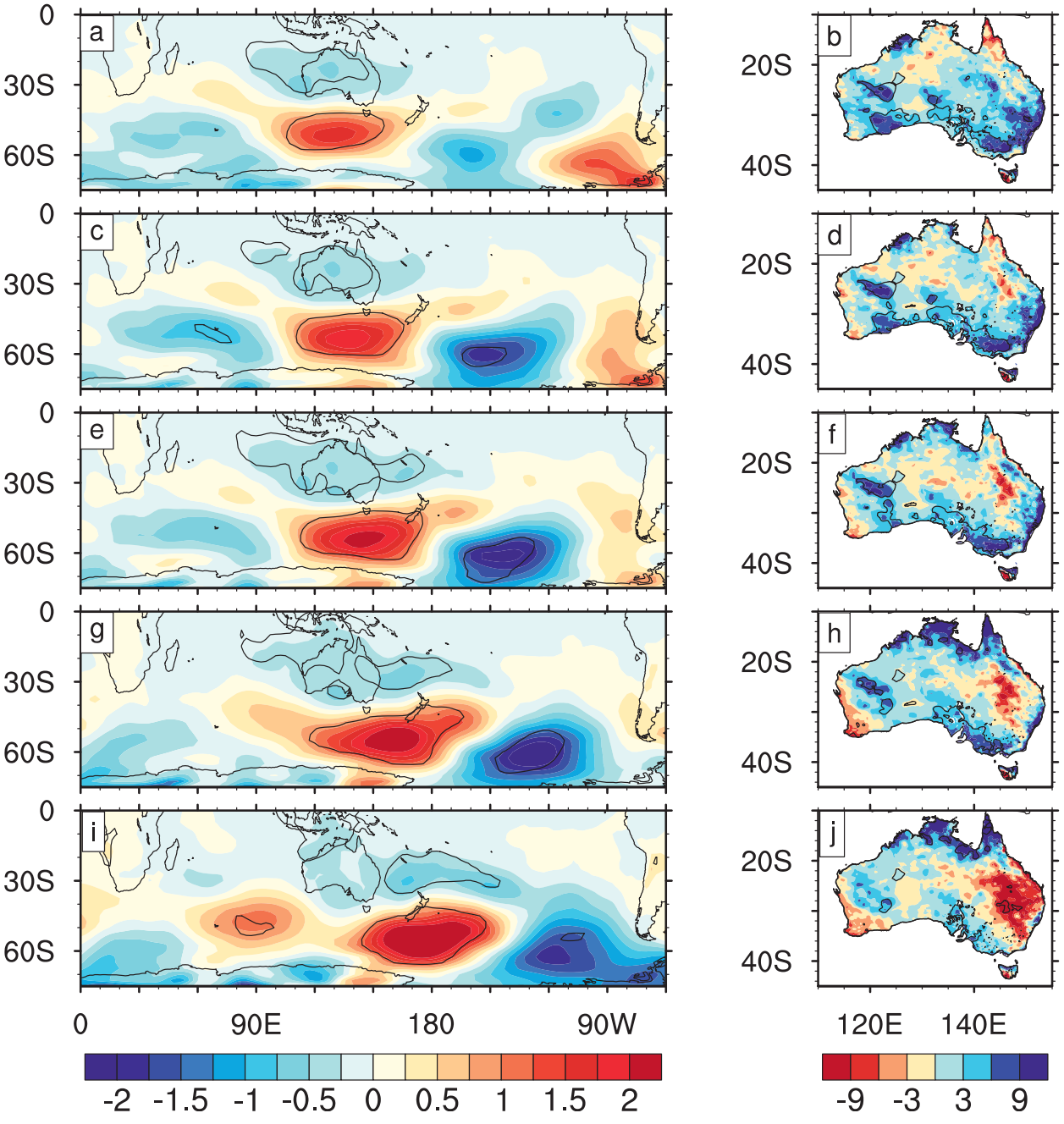

FIG. 2. April–May regression of (left) MSLP (hPa) and (right) Australian rainfall (mm month^{-1}) onto a blocking index B at (top to bottom) longitudes 120°–160°E at 10° intervals. Anomalies are shown as the one-standard-deviation anomaly of B. Contours encompass regression coefficients statistically significant at the 95% confidence level. Please note: the color legends for rainfall in this figure and all that follow are reversed (blue = positive rainfall anomalies).

low pressures across much of Australia (Figs. 2a,c,e). Despite the widespread continental low pressure anomalies, the corresponding anomalous rainfall increase is isolated to coastal SEA; no statistically significant rainfall anomaly is observed over southwest Australia (Figs. 2b,d,f). The greatest coherence is seen at 130°E (B130). As the blocking pattern moves east of 140°E, the impact on SEA's April–May rainfall diminishes (Figs. 2g–j). The pressure and rainfall anomalies across Australia associated with blocking suggest that both tropical and subtropical processes (e.g., cutoff lows) could potentially be important for SEA in this season (e.g., Cai and Cowan

TABLE 1. Autumn (April–May) correlations of blocking at 130°E, and winter (JJA) and spring (SON) correlations of blocking at 140°E with the DMI, Niño-3.4, and SAMI over 1979–2010. All indices are detrended prior to calculation. Bold numbers indicate significance above the 95% confidence level.

	April–May	JJA	SON
DMI	**−0.52**	−0.27	−0.19
Niño-3.4	−0.17	**−0.48**	−0.24
SAMI	0.03	0.11	**0.65**

2008a). That the agriculturally significant Mallee region (see Fig. 1a for location), known to be affected by cutoff lows in the cool season (Brown et al. 2009; Pook et al. 2009), is located where the strongest rainfall signal is observed further supports this hypothesis.

To elucidate the coherence between blocking and the climate modes, we first correlate B130, which shows the greatest coherence with April–May rainfall, with the three main modes (the IOD, ENSO, and SAM; see Table 1). Immediately it is clear that the B130-induced impact on April–May rainfall across SEA is not due to an influence from the SAM; the correlation between the SAMI and B130 is close to zero (0.03). Furthermore, the SAMI is not correlated with southern Australian rainfall in the autumn season (Meneghini et al. 2007; Hendon et al. 2007; Risbey et al. 2009b). Likewise, ENSO, as measured through the Niño-3.4, is only weakly correlated with B130, consistent with the lack of ENSO coherence with the local circulation over SEA during autumn (Cai et al. 2011b).

There is emerging evidence that, since the 1970s, IOD events are developing prematurely, that is, in mid to late autumn (April–May) (Du et al. 2013). In these two months there is a strong IOD–B130 coherence; the correlation of −0.52 (Table 1) is statistically significant. The negative correlation infers that circulation anomalies associated with positive blocking are coherent with those associated with a negative DMI. We therefore compare anomaly patterns of SST, 200-hPa geopotential height, moisture flux (integrated below 500 hPa), and Australian rainfall associated with B130, the DMI (× −1), and the residual ($\text{DMI}|_{\text{B130}}$; × −1) for April–May (Fig. 3). As mentioned in the previous section, to facilitate a more

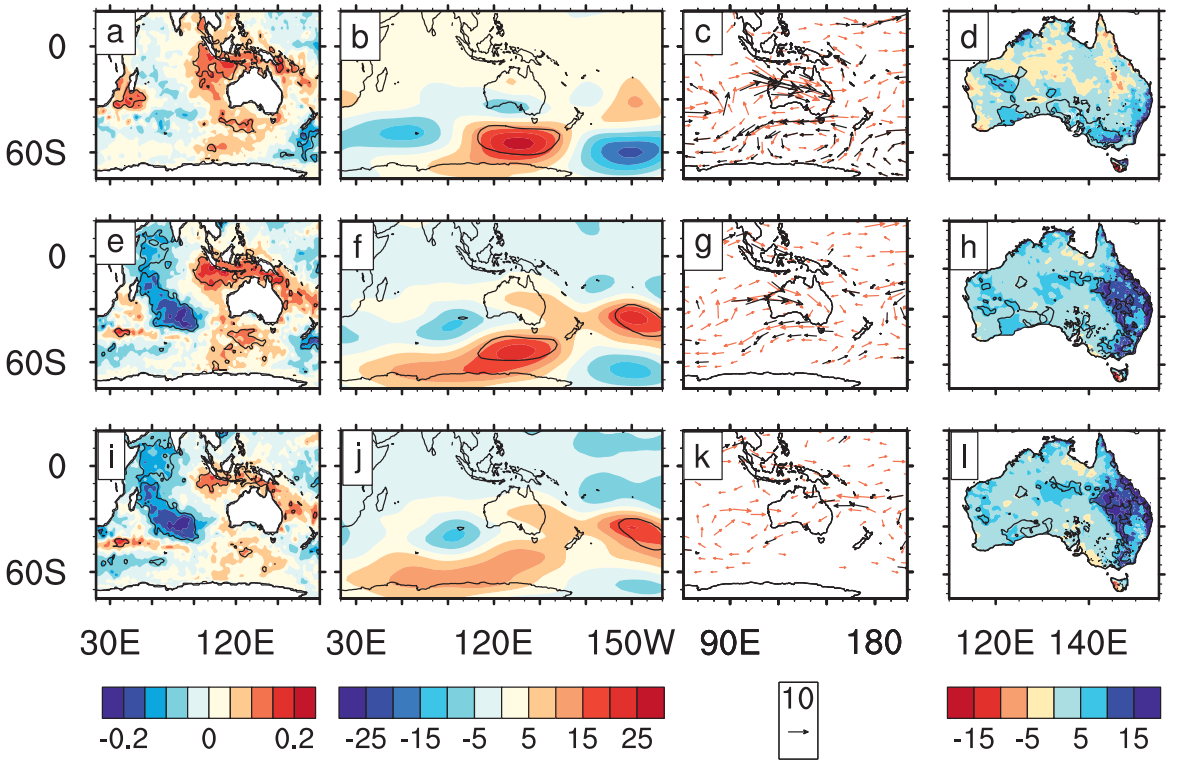

FIG. 3. April–May regression of (left to right) SST (°C), 200-hPa geopotential height (m), surface–500-hPa vertically integrated moisture flux (reference vector = 10 kg m^{-1} s^{-1}), and Australian rainfall (mm month^{-1}) onto (a)–(d) B130 (blocking at 130°E), (e)–(h) DMI, and (i)–(l) residual DMI (with B130 variations removed). The regression and correlation coefficients associated with the DMI and residual DMI are multiplied by −1 to take into account the association between positive blocking and negative IOD events. Contours and black vectors highlight regression coefficients statistically significant at the 95% confidence level.

direct comparison of the associated pattern of blocking to the IOD and ENSO, indices are sign reversed to reflect their negative coherence with B130.

Blocking and the IOD

The circulation anomalies associated with B130 include warm SST anomalies in the tropical eastern Indian Ocean and enhanced westerly moisture flux anomalies extending from this region (Figs. 3a,c, respectively). Anomalous easterly moisture fluxes are seen across southern Australia, straddling a positive height anomaly to the south (Fig. 3b); this reflects weak anomalous surface cyclonic circulation across southern Australia and an anomalous anticyclonic pattern to the south (Fig. 2c). The anomalous cyclonic circulation advects high tropical moisture anomalies to southern Australia first via enhancing the climatological westerly flow of moisture and then through the return of anomalous easterly moisture (in the mean state the moisture fluxes across southern Australia are westerly; Fig. 3c). The positive height anomaly, as part of the anticyclonic cell, weakens the climatological westerly flow (not shown) that leads to an increase in rainfall anomalies over the coastline regions of SEA (Fig. 3d).

Similar anomalous patterns are observed for the negative DMI (Figs. 3e–h). The associated SST anomaly pattern reflects a negative IOD phase (Fig. 3e) although the pole in the west tropical Indian Ocean extends into the subtropics, reminiscent of the subtropical SST dipole events observed in the austral summer (Behera and Yamagata 2001; Fauchereau et al. 2003). The anomalous positive height center is located due south of Australia (as for blocking; Fig. 3f). Enhanced westerly moisture advection is seen to extend from the subtropical eastern Indian Ocean (Fig. 3g), associated with pressure anomalies off western Australia. As in winter, a negative DMI is associated with an anomalous rainfall increase over SEA, but in April–May this increase extends farther north along eastern Australia's coastline (Fig. 3h), in part reflecting a coherence with eastern Indian Ocean SSTs and SSTs to the north of Australia (Cai and Cowan 2008a; Catto et al. 2012).

However, the process that delivers rainfall is somewhat different from that in JJA. In April–May, the mean westerly jet is still situated to the south of Australia, and the mean SST over the Tasman Sea region is high, conducive for convection; as such, the associated positive height anomaly center south of Australia (Fig. 3f) promotes anomalously weak easterly flows over the south Tasman Sea (Fig. 3g), leading to an increase in rainfall across southern SEA. Further north, the weak easterly flow over the Coral Sea provides a moisture source for central-eastern regions and the northeastern Australian coastline. In contrast, in JJA, negative IOD events that involve anomalous westerly moisture advection are the main process for delivering rainfall over SEA and the IOD's influence is conducted through modulating such weather events (Cai et al. 2011b,c).

Removing the covariance of B130 from the DMI substantially weakens the eastern tropical Indian Ocean SST anomalies, as well as the height and moisture flux anomalies to the south of Australia (Figs. 3i–k), further highlighting the strength of the DMI–B130 coherence. The removal of B130 from the DMI also leads to a slight weakening of the anomalous rainfall signal, particularly over the southern coastline of Australia (Fig. 3l), reflecting the fact that only a small part of the IOD's impact on rainfall across the southeast occurs through blocking events. When the blocking index is positive an anomalous anticyclonic cell over the ocean south of Australia allows for cutoff low systems to penetrate northeastward, generating early cool season rainfall to southern Australia. Despite this, the importance of the IOD in this season is not well understood. Whether the anomalous anticyclonic pressure center due south of Australia is generated in terms of a Rossby wave train signal (as in JJA and SON) emanating from the tropical eastern Indian Ocean is unclear; further investigation is required to understand the impacts of autumn IOD events and their prevalence (Du et al. 2013), as well as other autumnal subtropical IOD modes such as those described in Cai and Cowan (2008a, 2013).

4. Winter anomalies

A similar methodology as for April–May is conducted for JJA to identify the longitude with the highest coherence to SEA rainfall. For this season, once the blocking center goes eastward exceeding 160°E, the blocking–rainfall relationship diminishes across Australia (not shown). The winter blocking regime is somewhat different from that during April–May, with blocking at 140°E (B140) associated with larger, broader rainfall anomalies across eastern Australia, stretching northwestward (Fig. 4b). The associated high pressure anomaly pattern displays a ridge that is more zonally elongated across the midlatitudes than for April–May. Across the Australian tropics the MSLP pattern associated with B140 resembles the well-known SO pattern (Fig. 4a). As such, during winter ENSO and B140 are significantly negatively correlated (−0.48; see Table 1), reflecting the strong association of La Niña events with blocking in the austral winter.

For the IOD and SAM, their respective indices only show insignificant correlations with B140 in winter (Table 1). While a negative IOD tends to be more coherent with

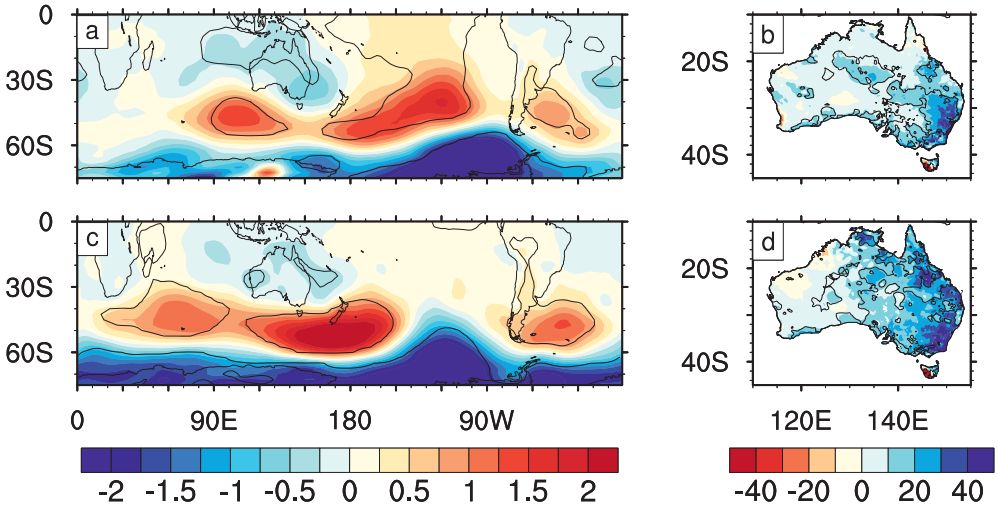

FIG. 4. (top) Austral winter and (bottom) austral spring regression of (left) MSLP (hPa) and (right) Australian rainfall (mm season^{-1}) onto a blocking index at 140°E (B140). Anomalies are shown as the one-standard-deviation anomaly of B140. Contours encompass regression coefficients statistically significant at the 95% confidence level.

positive blocking, only a small portion of the IOD's impact on SEA winter rainfall occurs through blocking events (not shown) because the negative height anomaly center associated with B140 is located equatorward of the height anomaly associated with the DMI (Fig. 4c of Cai et al. 2011b); this spatial mismatch leads to a weak correlation between B140 and the DMI (−0.27; Table 1). As the SAMI shows an even weaker correlation with B140 in winter (discussed in section 5), we only focus on the relationship of B140 and ENSO for JJA and test their respective impacts on SEA rainfall.

Blocking and ENSO

It is known that ENSO has very little impact on rainfall in the southern regions of SEA in winter (Cai et al. 2011c), despite the high correlation between the SOI and rainfall over other regions of Australia (Risbey et al. 2009b). The impact of ENSO on northeastern Australia stems from the tropically trapped Gill-type (baroclinic) response, manifested through the SO pattern. The extratropical response in the SH is through equivalent barotropic Rossby wave trains (the PSA pattern) that emanate from the central tropical Pacific; however, the midlatitude anomaly centers are situated too far east of Australia in JJA to impinge on the Australian east coast (Cai et al. 2011c).

Despite this, B140, which has an extratropical component, is highly coherent with ENSO in JJA (Table 1), and the associated anomalous circulation somewhat resembles a La Niña–like pattern in the tropics based on the 200-hPa geopotential height (Fig. 5a). Anomalous low pressure anomalies extend from the western tropical Pacific, and an anomalous closed cyclonic system is seen over Australia. This broad anomalous MSLP pattern over Australia is also seen in a composite of the seven largest La Niña events from 1979 to 2006 (not shown). This has the effect of directing anomalous high-moisture flow from tropical northern Australia and subtropical south Pacific to eastern and SEA (Fig. 5b), leading to positive rainfall anomalies over these regions (Fig. 5c). This anomalous cyclonic circulation pattern over Australia is accompanied by the more zonally elongated midlatitude high pressure anomaly center to the south that extends from the southern Indian Ocean across to the southern Pacific. Similar to April–May, a manifestation of the cyclonic and anticyclonic anomaly pair allows for anomalous moisture convergence across SEA (Fig. 5b). A similar pattern is seen for 500-hPa relative vorticity for cutoff low systems (Risbey et al. 2009a), and the anomalous moisture convergence is associated with large rainfall anomalies across southern Australia, particularly the southeast coast from a moisture source that originates in either the subtropical South Pacific or the northern tropics (Fig. 5c). Such moisture flux anomalies associated with blocking thus play an opposite role to the moisture regime unrelated to the blocking-induced cyclonic low pressure anomaly pattern. For example, easterly moisture flux anomalies associated with the SAM act to weaken the mean westerly weather systems, which are the dominant rainfall-generating process in winter (this is discussed in more detail in section 5).

The B140–La Niña coherence (Table 1) suggests that ENSO may exert an influence on, or is associated with, B140 such that it influences Australian winter rainfall.

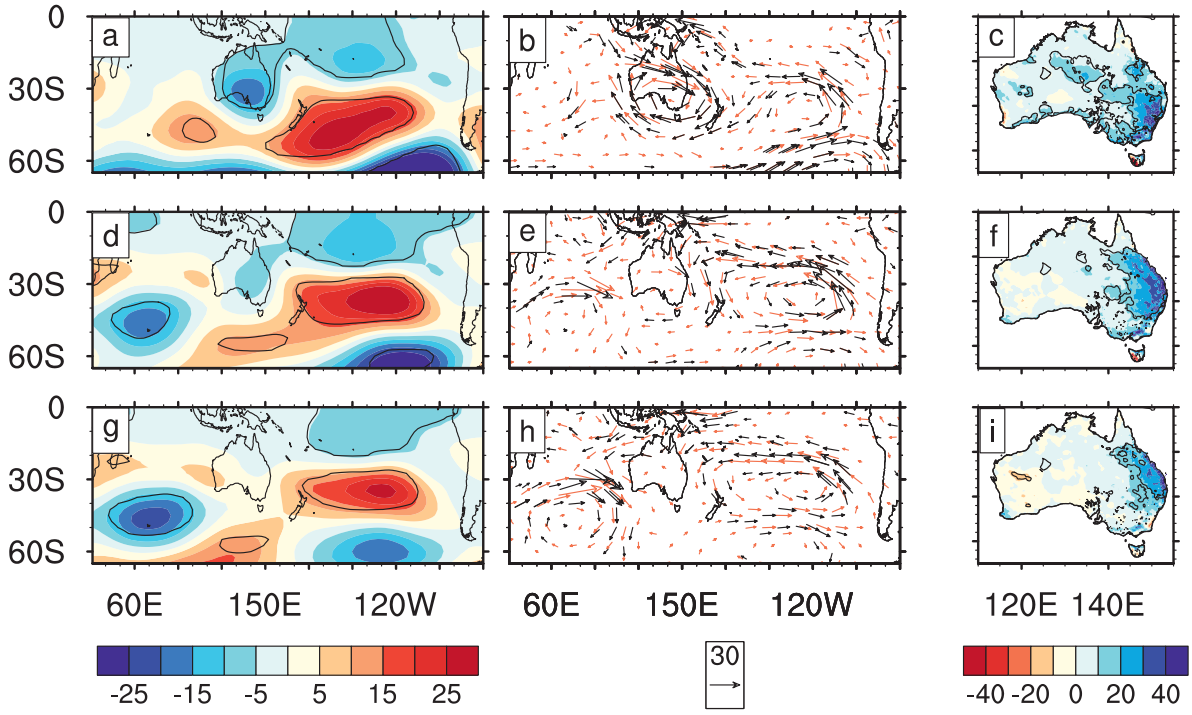

FIG. 5. Winter regression of (left) 200-hPa geopotential height (m), (middle) surface–500-hPa vertically integrated moisture flux (reference vector = 30 kg m^{-1} s^{-1}), and (right) Australian rainfall (mm season^{-1}) onto (a)–(c) B140, (d)–(f) Niño-3.4, and (g)–(i) residual Niño-3.4 (with B140 variations removed). The regression and correlation coefficients associated with the Niño-3.4 and residual Niño-3.4 are multiplied by −1 to take into account the association between positive blocking and La Niña (negative Niño-3.4). Contours and black vectors highlight regression coefficients statistically significant at the 95% confidence level.

Moist air off the coast of northeastern Australia can feed into cutoff low pressure systems (which often are associated with blocking), generating significant rainfall events across SEA, as seen in 1997 during an El Niño (Brown et al. 2009). There is a broad resemblance in the structures of the moisture flux anomalies associated with B140 and with La Niña (Figs. 5b,e), although the fluxes are much weaker over southern Australia in the La Niña case. La Niña events generate on-shore moisture flux anomalies toward eastern and northeastern Australia; circulation anomalies associated with blocking appear to circulate and redirect the moisture that has originated from the Pacific, affecting the rainfall distribution, including an influence on the northern part of SEA. The anomalously weak cyclonic flow over SEA associated with La Niña does not correspond to a rainfall signal for southern SEA. The B140–La Niña coherence mainly reflects the anomalous cyclonic-flow process. Figures 5d–f highlight circulation and Australian rainfall anomaly patterns associated with La Niña. To the east of Australia, the associated enhanced onshore advection provides a moisture source for eastern and northeastern Australia (Fig. 5e). This is similar to the process that led to significant high rainfall events across SEA in 1997 (Brown et al. 2009). This is a response to a positive SO during a La Niña, with only a very weak cyclonic circulation anomaly over eastern Australia (Fig. 5d).

Removing the covariant B140 signals results in weaker circulation over SEA, resulting in a weakening of the rainfall anomalies across the northern part of SEA (Figs. 5g–i). Without the redirection of moisture flux by B140, the associated rainfall anomalies are concentrated on the northeast, with no impact on southern Australia. This suggests that La Niña's impact on the southern regions of the Murray-Darling basin (see Fig. 1 for region) is modified by blocking; the subtropical component of B140 (moisture fluxes at 25°–30°S) enhances the rainfall response over eastern Australia, with its impact confined to the northern Murray-Darling basin (north of 32°S in SEA). Pure La Niña (with blocking removed) has very little effect on rainfall anomalies over southern regions of SEA (cf. Figs. 5f and 5i). The B140–La Niña relationship is consistent with previous findings (e.g., Risbey et al. 2009b), where it has been shown that La Niña is more strongly associated with positive blocking events than El Niño is with weak (negative) blocking. This asymmetry is seen when comparing the relative coherence of B140 with La Niña and El Niño (not shown).

5. Spring anomalies

It is during spring that blocking has the most widespread impact on Australian rainfall, at 140°E (Figs. 4c,d); the cyclonic anomaly center over Australia that is prominent in the winter season is weaker, but a more zonal and stronger high MSLP belt emerges to the south of Australia, with a pattern more closely resembling that of the SAM. The strong resemblance between blocking and the SAM in the MSLP pattern suggests that blocking is possibly a local manifestation of the SAM. The strength and significance of the resultant positive correlation (0.65; Table 1) also confirms the fact that blocking events coincide with the positive phase of the SAM.

For the IOD and ENSO, the spring correlations with B140 are weak, which again suggests that the circulation anomalies associated with these tropical modes do not align with the anomalous anticyclones to the south of Australia. Despite the weak correlations, B140 tends to strengthen the rainfall response of the IOD over northeast Australia and SEA (not shown). Given that the IOD has no direct pathway to impact northeast Australia, much of the seemingly B140-induced enhancement in fact reflects the coherence of B140 with ENSO. As detailed in Cai et al. (2011c), ENSO's impact on SEA is conducted through its strong coherence with the IOD in the spring. While ENSO has an impact on eastern Australia through the tropical response via the SO, removing the covariant B140 signals from ENSO does not weaken this tropical response of rainfall (not shown). Only a small portion of ENSO's extratropical impact is accounted for by blocking and comes via the tropical Indian Ocean. Thus, during spring the IOD and ENSO teleconnect much of their impacts on Australia through processes that are independent of blocking, such as by influencing the position of the local subtropical ridge across SEA (Cai et al. 2011b).

a. Blocking and the SAM

Although known for its zonally symmetric structure, the SAM pattern has embedded regional centers with significant regional flows in the upper troposphere (Fig. 6a). One such center is located in the southwest Pacific, where the anomalous onshore flows (for the positive SAM phase) provide a means by which moisture-laden air can penetrate SEA (Fig. 6b) and thus generate substantial rainfall anomalies (Fig. 6c). For northeast and northern Australia, enhanced northwesterly moisture flow, which forms part of a recirculation of moisture from the west Pacific, contributes to significant rainfall anomalies. The southwest Pacific regional high pressure center anomaly associated with the SAM coincides with a pressure anomaly that is associated with blocking. Thus, spring atmospheric blocking is in phase with the SAM in terms of their associated atmospheric and rainfall anomalies (cf. Figs. 6a–c and 6j–l). This is despite the weaker blocking-induced cyclonic anomaly center over Australia in spring compared with winter (cf. Figs. 4a and 4c). However, the moisture flow anomalies associated with blocking in spring (Fig. 6k) are similar to that in April–May (Fig. 3c) and winter (Fig. 5b). All exhibit an anomalous cyclonic–anticyclonic pairing, with anomalous easterly moisture fluxes over southern Australia; in spring, the anticyclonic anomaly forms part of the hemisphere-scale high MSLP anomaly ridge; this also resembles the anomalous pressure ridge associated with a positive SAM.

Once the impact of B140 is removed, little SAM signal remains in the circulation and rainfall anomaly patterns (Figs. 6d–f). That is, blocking events that enhance rainfall-generating processes tend to occur during positive SAM phases. Only a small part of the SAM signal is independent of blocking and vice versa (Figs. 6g–i). Removal of the impact of B140 leads to a diminishing influence of the two moisture sources from the Pacific (Fig. 6e): one from the tropical west Pacific that recirculates moisture toward northeastern Australia; the other from the subtropical South Pacific that influences SEA. Removal of the SAM's impact (from B140) leaves residual easterly moisture fluxes that are associated with isolated rainfall anomalies over coastal SEA (Figs. 6h,i). However, without the western tropical Pacific moisture source, the residual westerly moisture anomalies result in little change to rainfall across northern and central Australia. Despite this, it is not clear through what process circulation anomalies (associated with the SAM) generate the moisture recirculation from the western tropical Pacific in addition to the easterly moisture flux anomalies over central Australia.

During spring, blocking events in the vicinity of 140°E allow for the formation of cutoff lows during positive SAM phases, increasing the likelihood of anomalous onshore moisture flows from the southwest Pacific (Fig. 6k). In winter, a positive SAM leads to a reduced rainfall across southwest Australia (Cai and Cowan 2006; Hendon et al. 2007) and SEA (Hendon et al. 2007), as a result of easterly moisture anomalies weakening the mean westerly flow, which in turn weakens the westward progression of rain-bearing weather events.

Thus, in winter blocking and the SAM have an offsetting impact (discussed further in section 5b for the winter of 2010), whereas in spring the impact of blocking is to reinforce the effects of a positive SAM. This raises the question as to why blocking and SAM have such distinct impacts on rainfall between winter and spring.

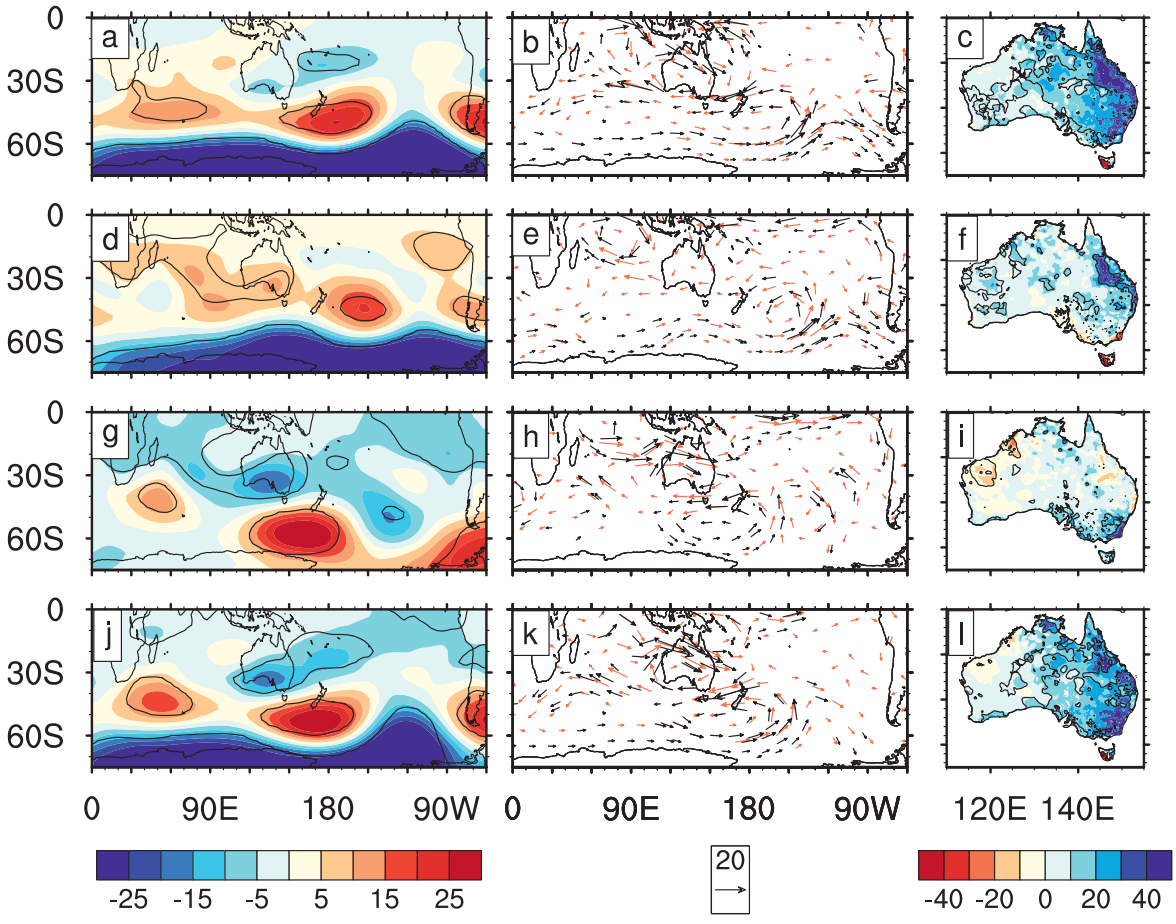

FIG. 6. Spring regression of (left) 200-hPa geopotential height (m), (middle) surface–500-hPa vertically integrated moisture flux (reference vector = 20 kg m^{-1} s^{-1}), and (right) Australian rainfall (mm season^{-1}) onto (a)–(c) SAMI, (d)–(f) residual SAMI (with B140 variations removed), (g)–(i) residual B140 (with SAMI variations removed), and (j)–(l) B140. Contours and black vectors highlight regression coefficients statistically significant at the 95% confidence level.

Figure 7 shows the anomalous zonal component of the moisture flux associated with B140 and the SAMI for winter and spring, as well as the Australian rainfall patterns associated with variations in the SAMI. Also shown is the mean location of the high pressure ridge (indicated by the dotted contour in Fig. 7) in both seasons. This blocking-induced ridge sits between 50° and 55°S and is straddled by anomalous easterly (westerly) moisture advection on the equatorward (poleward) side (Figs. 7a,d). In winter, the B140-induced wind regime reflects an anomalous cyclonic pressure circulation that brings high moisture from the tropics, first southward and then veering westward to the southern regions of SEA. The process is coherent with the conditions associated with a La Niña event. For the winter SAM, the position of the midlatitude pressure ridge is crucial in determining the rainfall response (Figs. 7b,c), and one can see that anomalous moisture patterns do not support the existence of an anomalous cyclonic cell (Fig. 7b), or that a source of tropical moisture is involved; the high-pressure ridge and anomalous easterly moisture flow that sit just north of Tasmania weaken the rain-producing westerly synoptic systems (Fig. 7c).

However, in spring the ridge and anomalous flow are situated farther poleward (Fig. 7e), aligning with the blocking-induced circulation anomalies (Fig. 7d); in this season the anomalous easterly flows are an important source of moisture (Fig. 7f), which are promoted by the anomalous on-shore flows associated with the SAM and blocking. The on-shore advection of moisture also allows for cutoff low formation to the south. Thus, during spring the impacts of the SAM and atmospheric blocking south of Australia are indistinguishable.

b. 2010 spring conditions over southern Australia

The extent to which atmospheric blocking can explain the climatic conditions in the cool season of 2010 across Australia is investigated. Rainfall anomalies in terms of

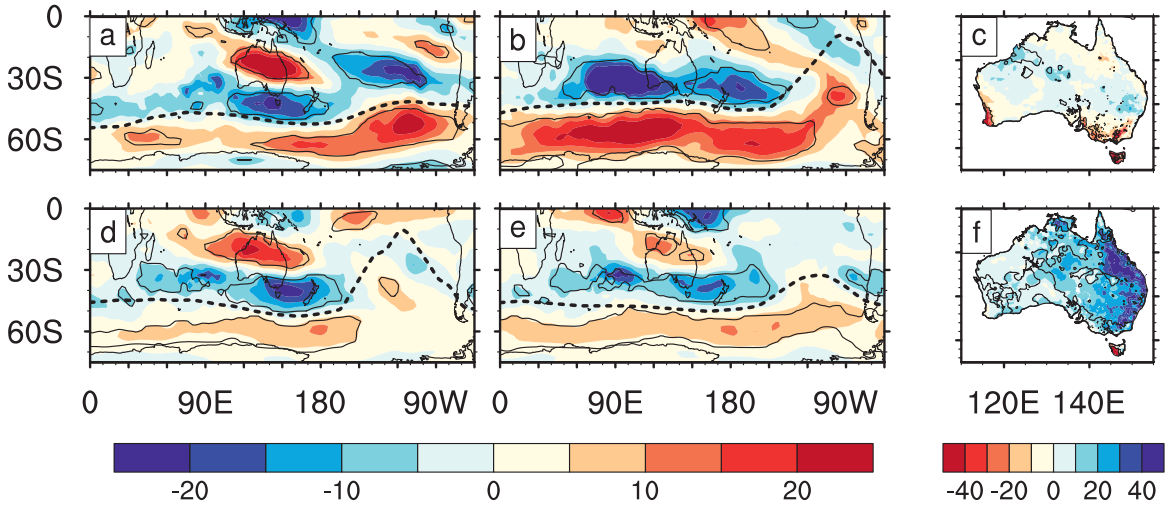

FIG. 7. (top) Winter and (bottom) spring regression of surface-500 hPa vertically integrated zonal moisture flux (kg m^{-1} s^{-1}) onto (left) B140 and (middle) SAMI, and (right) Australian rainfall (mm season^{-1}) associated with the SAMI. The dotted contour line in (left) and (middle) panels indicates the associated maximum MSLP ridge, while the solid lines in all panel contours encompass regression coefficients statistically significant at the 95% confidence level.

a percentage of climatology for April–May, JJA, and SON for 2010 are shown in Fig. 8, along with climate index values. One can immediately see that the substantial rainfall anomaly for the cool season total (Fig. 1a) is predominantly due to spring anomalies (Fig. 8c). In April–May, while blocking, SAM, and ENSO are all weak, the DMI signal is stronger (greater than the one-standard-deviation value), with the anomalous rainfall response across SEA predominantly drier than average (Fig. 8a).

The situation in winter is quite different (Fig. 8b), with a strong blocking value (more than 3 times the one-standard-deviation value), the emergence of a negative IOD, and a developing La Niña event, all inducing wetter than average conditions across SEA. However, the SAM was extremely positive (a record value; see Cai et al. 2011a), leading to a record dry winter over southwest Australia, and potentially offsetting the "wettening" impact on SEA from the combination of a negative IOD, a La Niña, and strong seasonal blocking. As a result, winter rainfall over SEA is close to the long-term average (Fig. 8b).

In spring, the blocking substantially weakened, despite the strength and significance of the other climate mode indices. This weakening is likely due to the strong seasonality of blocking, which peaks in winter (Pook and Gibson 1999). The strong SAM persisted, while the IOD and ENSO stayed in their negative phases, favoring wetter than average conditions for eastern Australia and SEA. Surprisingly, despite the strong SAM, there was no commensurably strong seasonal blocking, which in fact recorded a weak negative value, tending to offset the rain-inducing effects associated with the three climate mode indices. The fact that the strongest rainfall signals were observed across tropical eastern Australia suggests that the wet conditions occurred despite the unfavorable state of blocking index.

6. Summary and conclusions

Using observational and reanalysis data we have investigated the relationship between atmospheric blocking to the south of Australia and the three main climate modes that influence Australian rainfall: the IOD, ENSO, and SAM. While the purpose of this study was to examine whether these climate modes project their influence on southern Australian cool season rainfall (mid to late autumn, winter, and spring) through blocking events, we mainly focused on SEA where the agriculturally important Murray-Darling basin is located.

For April–May, only the IOD and blocking exhibit a statistically significant relationship; during this season, despite its influence being restricted to southern SEA, anomalous circulation patterns associated with blocking feature a high pressure center south of Australia, with easterly moisture flux anomalies conducive to rainfall over SEA. This feature is seen when a negative IOD event is in its development stage, which has been observed to occur more frequently since the 1970s (Du et al. 2013). The extent to which the recent multidecade-long expansion of the subtropical dry zone in late autumn (e.g., Hu and Fu 2007) has impacted recent blocking is not

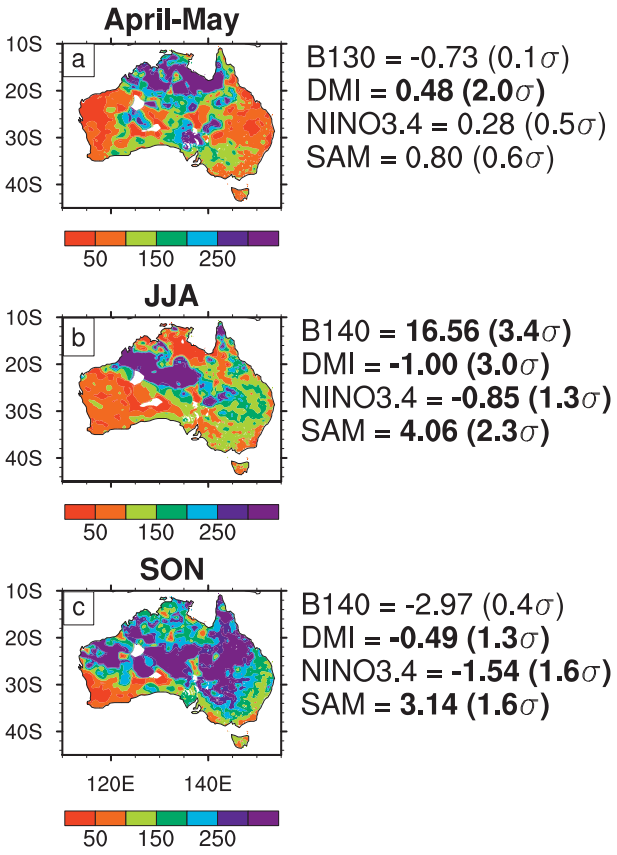

FIG. 8. Anomalies of Australian rainfall (% of climatology) over 2010 for (a) April–May, (b) JJA, and (c) SON. All anomalies are referenced to the 1971–2000 climatological period, with orange–red (light–dark blue) color indicating below (above) average rainfall. Also given are the 2010 values of the climate mode indices with their respective number of sigmas (σ); absolute values $> 1\sigma$ are in bold.

yet clear. Risbey et al. (2009b) suggest that since the late 1970s atmospheric blocking has been stronger and broader in scale. This has coincided with a both a decrease and a delay in the autumn break (first rainfall of the winter season) for SEA, which is predominately due to a reduction in active cutoff lows during the mid-1990s (Pook et al. 2009).

In winter, coherence between ENSO and blocking is statistically significant, with blocking reinforcing the tropically induced impact on rainfall in northern SEA through the direct SO teleconnection. In contrast, the impact of blocking is opposite to the SAM-induced drying influence. Although the associated circulation anomalies both feature easterlies over southern Australia, their function is also opposite: blocking delivers moisture and rainfall from the tropics to SEA, while the SAM weakens the westerly weather systems that deliver rainfall to the region. The tropical influence delivered via winter blocking events can be traced to a cyclonic pattern over Australia that forms a part of the SO pattern associated with La Niña. This is consistent with the notion that La Niña's impact on eastern Australia is generated through the SO, of which blocking is strongly coherent, while the IOD's impact on SEA comes via equivalent barotropic wave trains (Cai et al. 2011c).

Toward the end of the cool season (spring) ENSO becomes highly coherent with the IOD and influences SEA via wave trains emanating from the tropical Indian Ocean. A direct coherence between blocking and ENSO is essentially absent. The SAM is associated with an anomalous pressure ridge farther poleward than in winter and becomes aligned with the blocking-induced extratropical circulation response. A positive SAM phase now promotes onshore moist flows to much of eastern Australia. Blocking no longer offsets the SAM-induced drying as for winter, but enhances the rainfall response over SEA by promoting onshore subtropical flows and increasing the tendency for cutoff lows to form across southern Australia (the blocking-induced high pressure is closer to southern Australia). In 2010, the occurrence of the three climate modes each at a phase conducive to rainfall over Australia allowed for the formation of nearly "perfect" climatic conditions for rainfall generation, particularly for southeast and eastern Australia. However, the weak atmospheric blocking did not play a part in inducing the record springtime rainfall totals for eastern Australia.

It should be noted that the results shown in this study assume linearity in all the regression relationships—that is, that the impacts of El Niño and La Niña (or positive and negative SAM or IOD phases) are equal. Recent research suggests that nonlinearities exist in the teleconnection of climate modes on regional rainfall (Ummenhofer et al. 2011; Cai et al. 2012). The extent to which these asymmetries influence blocking, particularly the positive phase of the SAM in spring, are still to be investigated. Another aspect to note is that these relationships are most likely influenced by multidecadal variability, as observed in the role of the IOD during SEA wet and dry periods (Ummenhofer et al. 2009, 2011). It is not clear how these relationships may change in a warming world given the uncertainty in the variability and mean-state changes in the Pacific and Indian Ocean (e.g., Collins et al. 2010). These issues offer important avenues for further research.

Acknowledgments. This research is supported by the Goyder Institute and the Australian Climate Change Science Program (ACCSP). The authors thank the internal reviews given by Evan Weller and Simon Borlace, and three anonymous reviewers for their comments and suggestions, which greatly improved the manuscript.

REFERENCES

Arblaster, J. M., and G. A. Meehl, 2006: Contributions of external forcings to southern annular mode trends. *J. Climate,* **19,** 2896–2905.

Ashok, K., Z. Guan, and T. Yamagata, 2003: Influence of the Indian Ocean dipole on the Australian winter rainfall. *Geophys. Res. Lett.,* **30,** 1821, doi:10.1029/2003GL017926.

Behera, S. K., and T. Yamagata, 2001: Subtropical SST dipole events in the southern Indian Ocean. *Geophys. Res. Lett.,* **28,** 327–330.

Brown, J. N., P. C. McIntosh, M. J. Pook, and J. S. Risbey, 2009: An investigation of the links between ENSO flavors and rainfall processes in southeastern Australia. *Mon. Wea. Rev.,* **137,** 3786–3795.

Cai, W., and T. Cowan, 2006: SAM and regional rainfall in IPCC AR4 models: Can anthropogenic forcing account for southwest Western Australian winter rainfall reduction? *Geophys. Res. Lett.,* **33,** L24708, doi:10.1029/2006GL028037.

——, and ——, 2008a: Dynamics of late autumn rainfall reduction over southeastern Australia. *Geophys. Res. Lett.,* **35,** L09708, doi:10.1029/2008GL033727.

——, and ——, 2008b: Evidence of impacts from rising temperature on inflows to the Murray-Darling basin. *Geophys. Res. Lett.,* **35,** L07701, doi:10.1029/2008GL033390.

——, and ——, 2013: Southeast Australia autumn rainfall reduction: A climate-change-induced poleward shift of ocean–atmosphere circulation. *J. Climate,* **26,** 189–205.

——, and P. van Rensch, 2013: Austral summer teleconnections of Indo-Pacific variability: Their nonlinearity and impacts on Australian climate. *J. Climate,* **26,** 2796–2810.

——, P. H. Whetton, and D. J. Karoly, 2003: The response of the Antarctic Oscillation to increasing and stabilized atmospheric CO_2. *J. Climate,* **16,** 1525–1538.

——, T. Cowan, and A. Sullivan, 2009: Recent unprecedented skewness towards positive Indian Ocean dipole occurrences and its impact on Australian rainfall. *Geophys. Res. Lett.,* **36,** L11705, doi:10.1029/2009GL037604.

——, P. van Rensch, S. Borlace, and T. Cowan, 2011a: Does the southern annular mode contribute to the persistence of the multidecade-long drought over southwest Western Australia? *Geophys. Res. Lett.,* **38,** L14712, doi:10.1029/2011GL047943.

——, ——, and T. Cowan, 2011b: Influence of global-scale variability on the subtropical ridge over southeast Australia. *J. Climate,* **24,** 6035–6053.

——, ——, ——, and H. H. Hendon, 2011c: Teleconnection pathways of ENSO and the IOD and the mechanisms for impacts on Australian rainfall. *J. Climate,* **24,** 3910–3923.

——, ——, ——, and ——, 2012: An asymmetry in the IOD and ENSO teleconnection pathway and its impact on Australian climate. *J. Climate,* **25,** 6318–6329.

Catto, J. L., N. Nicholls, and C. Jakob, 2012: North Australian sea surface temperatures and the El Niño–Southern Oscillation in observations and models. *J. Climate,* **25,** 5011–5029.

Collins, M., and Coauthors, 2010: The impact of global warming on the tropical Pacific Ocean and El Niño. *Nat. Geosci.,* **3,** 391–397.

Du, Y., W. Cai, and Y. Wu, 2013: A new type of the Indian Ocean dipole since the mid-1970s. *J. Climate,* **26,** 959–972.

Fauchereau, N., S. Trzaska, Y. Richard, P. Roucou, and P. Camberlin, 2003: Sea-surface temperature co-variability in the southern Atlantic and Indian Oceans and its connections with the atmospheric circulation in the Southern Hemisphere. *Int. J. Climatol.,* **23,** 663–677.

Frederiksen, J. S., and C. S. Frederiksen, 2007: Interdecadal changes in Southern Hemisphere winter storm track modes. *Tellus,* **59A,** 599–617.

Grose, M. R., M. J. Pook, P. C. McIntosh, J. S. Risbey, and N. L. Bindoff, 2012: The simulation of cutoff lows in a regional climate model: Reliability and future trends. *Climate Dyn.,* **39,** 445–459.

Hendon, H. H., D. W. J. Thompson, and M. C. Wheeler, 2007: Australian rainfall and surface temperature variations associated with the Southern Hemisphere annular mode. *J. Climate,* **20,** 2452–2467.

Hill, K. J., A. Santoso, and M. H. England, 2009: Interannual Tasmanian rainfall variability associated with large-scale climate modes. *J. Climate,* **22,** 4383–4397.

Hope, P., W. Drosdowsky, and N. Nicholls, 2006: Shifts in the synoptic systems influencing southwest Western Australia. *Climate Dyn.,* **26,** 751–764.

Hu, Y., and Q. Fu, 2007: Observed poleward expansion of the Hadley circulation since 1979. *Atmos. Chem. Phys.,* **7,** 5229–5236.

Jones, D. A., W. Wang, and R. Fawcett, 2009: High-quality spatial climate data-sets for Australia. *Aust. Meteor. Oceanogr. J.,* **58,** 233–248.

Kalnay, E., and Coauthors, 1996: The NCEP/NCAR 40-Year Reanalysis Project. *Bull. Amer. Meteor. Soc.,* **3,** 437–471.

Karoly, D. J., 1989: Southern Hemisphere circulation features associated with El Niño–Southern Oscillation events. *J. Climate,* **2,** 1239–1252.

Marshall, G. J., 2003: Trends in the southern annular mode from observations and reanalyses. *J. Climate,* **16,** 4134–4143.

McBride, J. L., and N. Nicholls, 1983: Seasonal relationships between Australian rainfall and the Southern Oscillation. *Mon. Wea. Rev.,* **111,** 1998–2004.

Meneghini, B., I. Simmonds, and I. N. Smith, 2007: Association between Australian rainfall and the southern annular mode. *Int. J. Climatol.,* **27,** 109–121.

Murphy, B. F., and B. Timbal, 2008: A review of recent climate variability and climate change in southeastern Australia. *Int. J. Climatol.,* **28,** 859–879.

Nicholls, N., 1989: Sea surface temperature and Australian winter rainfall. *J. Climate,* **2,** 965–973.

——, 2010: Local and remote causes of the southern Australian autumn-winter rainfall decline, 1958–2007. *Climate Dyn.,* **34,** 835–845, doi:10.1007/s00382-009-0527-6.

——, B. Lavery, C. Frederiksen, and W. Drosdowsky, 1996: Recent apparent changes in relationships between the El Niño Southern Oscillation and Australian rainfall and temperature. *Geophys. Res. Lett.,* **23,** 3357–3360.

Pook, M., and T. Gibson, 1999: Atmospheric blocking and storm tracks during SOP-1 of the FROST project. *Aust. Meteor. Mag.,* **1,** 51–60.

——, P. McIntosh, and G. Meyers, 2006: The synoptic decomposition of cool-season rainfall in the southeastern Australian cropping region. *J. Appl. Meteor. Climatol.,* **45,** 1156–1170.

——, S. Lisson, J. Risbey, C. C. Ummenhofer, P. McIntosh, and M. Rebbeck, 2009: The autumn break for cropping in southeast Australia: Trends, synoptic influences and impacts on wheat yield. *Int. J. Climatol.,* **29,** 2012–2026.

——, J. Risbey, and P. McIntosh, 2010: East coast lows, atmospheric blocking and rainfall: A Tasmanian perspective. *IOP Conf. Ser.: Earth Environ. Sci.,* **11,** 012011, doi:10.1088/1755-1315/11/1/012011.

Pui, A., A. Sharma, A. Santoso, and S. Westra, 2012: Impact of the El Niño–Southern Oscillation, Indian Ocean dipole,

and southern annular mode on daily to subdaily rainfall characteristics in east Australia. *Mon. Wea. Rev.,* **140,** 1665–1682.

Rayner, N. A., D. E. Parker, E. B. Horton, C. K. Folland, L. V. Alexander, D. P. Rowell, E. C. Kent, and A. Kaplan, 2003: Global analyses of sea surface temperature, sea ice, and night marine air temperature since the late nineteenth century. *J. Geophys. Res.,* **108,** 4407, doi:10.1029/2002JD002670.

Risbey, J. S., M. J. Pook, P. C. McIntosh, C. C. Ummenhofer, and G. Meyers, 2009a: Characteristics and variability of synoptic features associated with cool season rainfall in southeastern Australia. *Int. J. Climatol.,* **29,** 1595–1613.

——, ——, ——, M. C. Wheeler, and H. H. Hendon, 2009b: On the remote drivers of rainfall variability in Australia. *Mon. Wea. Rev.,* **137,** 3233–3253.

Saji, N. H., B. N. Goswami, P. N. Vinayachandran, and T. Yamagata, 1999: A dipole mode in the tropical Indian Ocean. *Nature,* **401,** 360–363.

Thompson, D. W. J., and J. M. Wallace, 2000: Annular modes in the extratropical circulation. Part I: Month-to-month variability. *J. Climate,* **13,** 1000–1016.

——, and S. Solomon, 2002: Interpretation of recent Southern Hemisphere climate change. *Science,* **296,** 895–899.

Timbal, B., and H. Hendon, 2011: The role of tropical modes of variability in recent rainfall deficits across the Murray-Darling basin. *Water Resour. Res.,* **47,** W00G09, doi:10.1029/2010WR009834.

Trenberth, K. E., and K. C. Mo, 1985: Blocking in the Southern Hemisphere. *Mon. Wea. Rev.,* **113,** 3–21.

Ummenhofer, C. C., M. H. England, P. C. McIntosh, G. A. Meyers, M. J. Pook, J. S. Risbey, A. S. Gupta, and A. S. Taschetto, 2009: What causes Southeast Australia's worst droughts? *Geophys. Res. Lett.,* **36,** L04706, doi:10.1029/2008GL036801.

——, and Coauthors, 2011: Indian and Pacific Ocean influences on southeast Australian drought and soil moisture. *J. Climate,* **24,** 1313–1336.

Wright, W. J., 1994: Seasonal climate summary Southern Hemisphere (autumn 1993): A second mature ENSO phase. *Aust. Meteor. Mag.,* **43,** 205–221.

Yin, J. H., 2005: A consistent poleward shift of the storm tracks in simulations of 21st century climate. *Geophys. Res. Lett.,* **32,** L18701, doi:10.1029/2005GL023684.